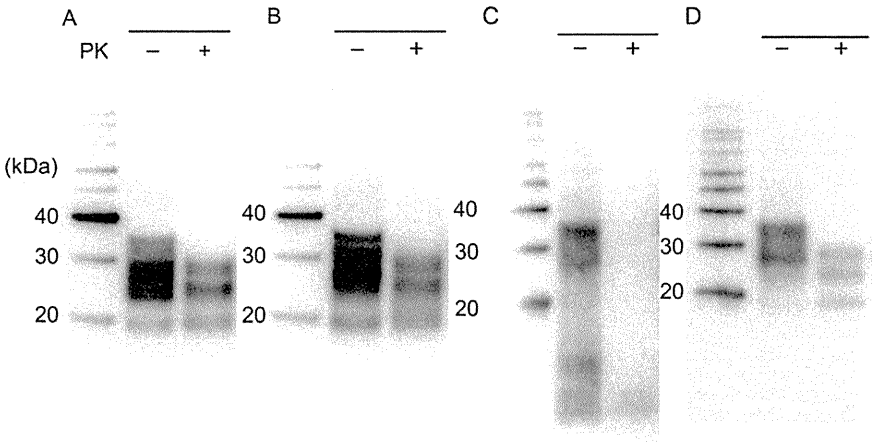

Fig. 3 Western blot analysis for PrP with or without proteinase K (PK) treatment. The brain homogenates from frontal cortices of pentosan polysulfate positive (PPS(+)) cases were separated by SDS-PAGE and probed with anti-PrP antibody (clone 3F4). The blot shows a type 1 pattern of PrP^{res} in case 1 (A) and case 2 (B). Case 3 shows PrP^{res} fragments with molecular masses of around 8 kDa (C). Case 4 shows PrP^{res} fragments with intermediate size between types 1 and 2 (D).

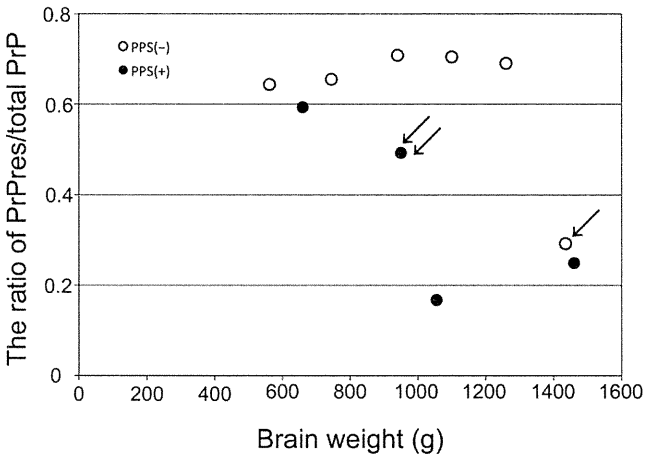

Fig. 4 Relationship between PrP^{res}/total PrP ratio and brain weight. The ratios of PrP^{res}/total PrP are markedly increased in all pentosan polysulfate negative (PPS(–)) cases (open circles) except for case 10 (arrow). Among PPS(+) cases (closed circles), case 2 (double arrows) shows a relatively low ratio of PrP^{res}/total PrP in comparison to PPS(–) cases.

atrophy. Case 2, one of three CJD cases with PPS(+), showed a relatively low ratio of PrP^{res}/total PrP in comparison to PPS(–) cases (Fig. 4).

The indices of oligomeric PrP/total PrP and monomeric PrP/total PrP

The first fraction consisted mostly of the void volume and contained insufficient protein to be assessed. Pre-column samples were taken as loading samples of total PrP. The aggregated forms of PrP were detected in fractions 2–4 (Fig. 5). Fraction 3 in this method represented the oligomeric PrP.[19,22] Thus, the index of oligomeric PrP/total PrP was obtained by dividing the intensity of fraction 3 by the intensity of the pre-column sample. Proteins with molecular weights of approximately 30 kDa, such as monomer PrP molecules, were collected mainly in fractions 6–8.[19,22] Fraction 7 represented the monomeric PrP. The index of monomeric PrP/total PrP was obtained by dividing the intensity of fraction 7 by the intensity of pre-column samples. In PPS(–) cases, the indices of oligomeric PrP/total PrP were increased according to the disease severity (Fig. 6A). Among PPS(+) cases, two CJD cases (cases 1 and 2) showed lower indices of oligomeric PrP/total PrP in comparison to PPS(–) cases. The indices of monomeric PrP/total PrP were decreased markedly in the cases with severe brain weight loss (Fig. 6B). There were no significant differences in the monomer indices between PPS(+) cases and PPS(–) cases.

DISCUSSION

Our post mortem study revealed that the PPS treatment did not apparently improve brain pathology in human prion diseases, although PPS treatment decreased the ratios of PrP^{res}/total PrP and the indices of oligomeric PrP/total PrP in some CJD cases. These findings might be relevant to apparently discrepant clinical findings: one reported no significant clinical improvements in prion diseases with PPS treatment[14,23] and the other reported that longer mean survival time in patients that had received PPS treatment was longer than previously reported for untreated specific prion diseases.[15]

The post mortem examinations revealed that neuronal loss, spongiform change and gliosis were advanced in both PPS(–) and PPS(+) cases with a greater loss of brain weight. In all PPS(+) cases, astrocytosis was evident in all layers of cerebral cortices, but GFAP expression levels were markedly reduced in the cerebral cortices, except in subpial astrocytes. CJD cases without PPS treatment usually showed strong immunoreactivity for GFAP in the cortical astrocytes as observed in case 5. Thus, we treated rat primary astrocytes with several concentrations of PPS (0 μg/mL, 0.4 μg/mL, 2.0 μg/mL, 10 μg/mL), but GFAP

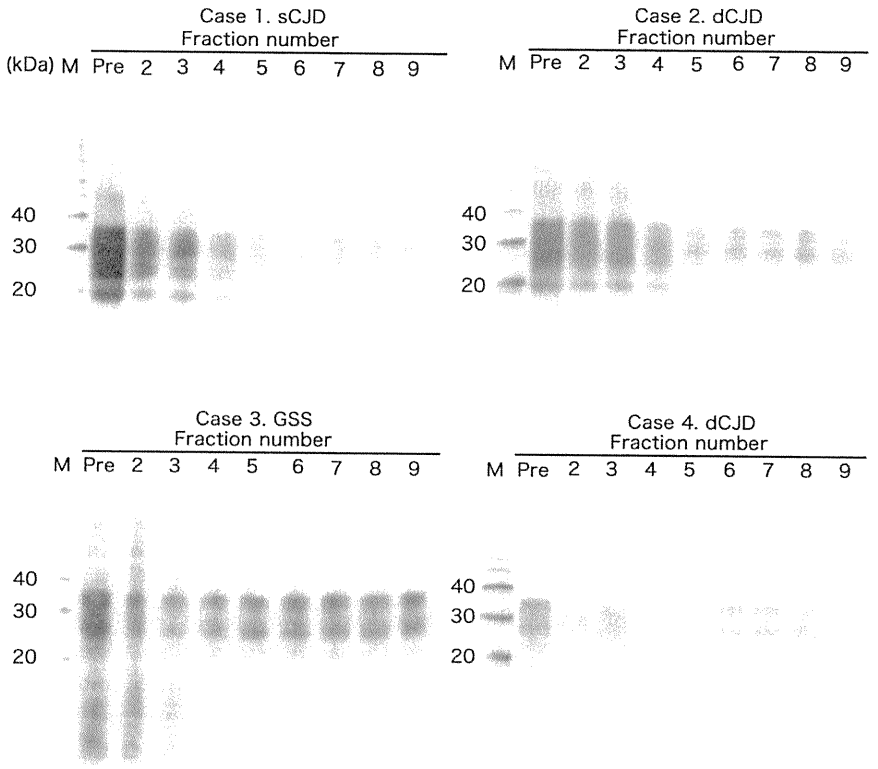

Fig. 5 Fractionation patterns of PrP in prion disease cases treated with PPS. The brain homogenate from the frontal cortex of each case was gel-filtrated without proteinase K (PK) treatment. Oligomeric PrP are detected mainly in fractions 2–4. Monomeric PrP are detected mainly in fractions 6–8. Pre: Pre-column brain homogenate.

expression levels were not significantly altered (data not shown). Therefore, we suggest that decreased GFAP expression levels in cortical astrocytes in PPS(+) cases is not due to the direct action of PPS on astrocytes.

PPS(+) cases in our study included only one case of sCJD (case 1). Although PPS infusion was started 3 months after disease onset, case 1 did not show any improvement in clinical features and the ratio of PrP^{res}/total PrP was comparable with PPS(−) sCJD cases. Meanwhile, two PPS(+) cases (cases 2 and 3) showed a relatively low ratio of PrP^{res}/total PrP. Because case 2 (dCJD) showed synaptic-type PrP deposition and type 1 PrP^{res} accumulation, it was considered to be a referential case to compare with PPS(−) CJD cases. Terada *et al.* also reported a reduction of PrP^{res} in a sCJD brain with PPS treatment.[23] In case 3 with GSS, PrP^{res} signals were very faint. It is possible that the molecular weights of plaque-type PrP deposition were too large to be detected through electrophoresis in these gels. Parchi *et al.* reported that immunoblot analysis of GSS P102L patients showed two major PrP^{res} signals with molecular masses of 21 and 8 kDa, and that the GSS patients with only the 8 kDa fragment showed mainly plaque-type PrP deposition.[24] In our study, the GSS patient with a P102L mutation showed both plaque-type PrP deposition and synaptic deposition, although Western blotting with PK treatment showed only PrP^{res} around 8 kDa. In this case, PrP^{res} might have a low resistance to PK treatment. Therefore, it may not be appropriate to compare the ratio of PrP^{res}/total PrP of case 3 to those of PPS(−) CJD cases. In case 4 with dCJD with plaque-type PrP deposits, Western blot analysis detected PrP^{res} fragments with intermediate size between types 1 and 2. Kobayashi *et al.* reported that the intermediate type PrP^{res} was seen in all examined dCJD cases with 129 methionine/methionine and plaque-type PrP deposits.[25]

Among PPS(+) cases, cases 1 and 2 showed lower indices of oligomeric PrP/total PrP than the indices of PPS(−) cases. PPS treatment might have reduced oligomeric PrP by reducing PrP^{res}. Alternatively, another study has reported that PrP fragments form amyloid aggregates in the presence of heparin which has a similar effect to PPS.[26] Therefore, oligomeric PrP in PPS(+) may be accumulated into fibrils. In our study, we did not evaluate fibrils because fibrils are difficult to electrophorese. Contrary to the reduction of oligomeric PrP/total PrP indices, monomeric PrP/total PrP indices in PPS(+) cases showed similar values to PPS(−) cases. The indices of monomeric PrP/total PrP were decreased, especially in cases with a brain weight of less than 1000 g. In these cases, PrP^{c} may have been depleted because of severe neuronal loss. Recently, oligomeric PrP was reported as the most infectious unit[17] and another study suggested that oligomeric PrP specifically inhibits the 26S proteasome, thus mediating a mechanism for intracellular neurotoxicity.[18]

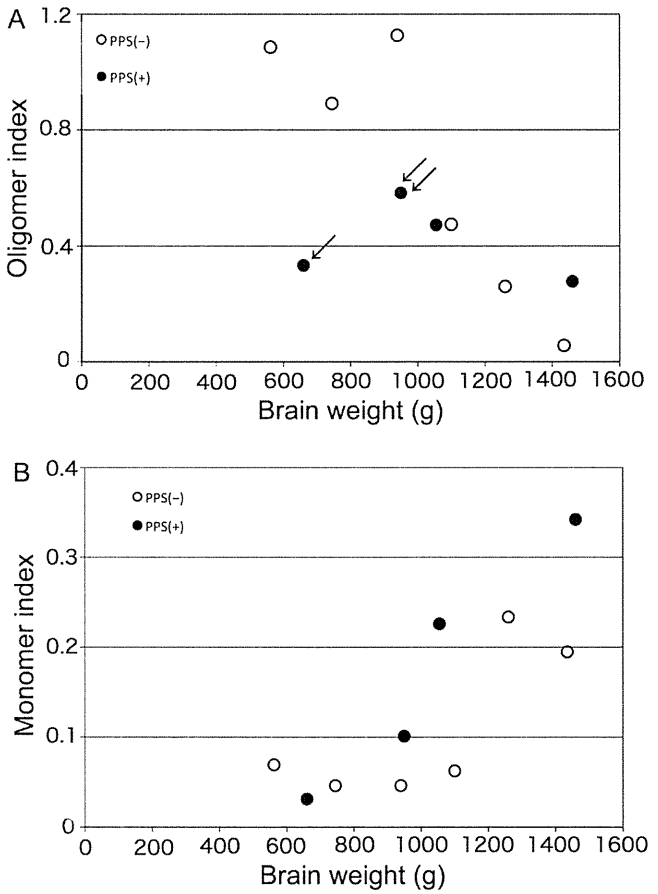

Fig. 6 Relationship between oligomeric PrP/total PrP indices and brain weight (A), or between monomeric PrP/total PrP indices and brain weight (B). (A) The oligomeric PrP/total PrP index was calculated by comparing the signals of fraction 3 to the signals of pre-column samples. In pentosan polysulfate negative (PPS(−)) cases (open circles), the oligomeric/total PrP indices are increased in accordance with brain weight loss. This tendency is also found in the PPS(+) cases (closed circles). The oligomeric PrP/total PrP indices in the PPS(+) cases are relatively low, particularly in the advanced cases with severe brain atrophy (case 1 (arrow) and case 2 (double arrows)). (B) The monomeric PrP/total PrP indices were calculated by comparing the signals of fraction 7 to the signals of pre-column samples. Monomeric PrP/total PrP indices of the advanced cases with severe brain atrophy are decreased irrespective of PPS treatment.

Doh-ura *et al.* reported that PPS infusion not only decreased PrP deposition but also reduced neurodegenerative changes in a rodent model.[9] However, in the rodent model PPS treatment could be started at the preclinical stage, whereas PPS treatment for patients was usually started at an advanced clinical stage. In the animal model, PPS treatment at an early or a late preclinical stage of the infection prolonged the incubation time by 2.4 or 1.7 times that of the control mice. Furthermore, the dosage of PPS in the animal model (460 μg/kg/day) was higher than the dosage for the human cases (120 μg/kg/day at a maximum).[9] Thus, if we could start PPS treatment at an earlier clinical stage or administer prophylactic PPS, the treatment might have beneficial effects on patients with prion diseases as shown in the experimental animal model.[9] Indeed the low indices of oligomeric PrP/total PrP were detected in two cases, but these cases showed no apparent clinicopathological improvements. Therefore, the therapeutic effects of intraventricular PPS infusion for human prion diseases are still uncertain.

ACKNOWLEDGMENTS

This work was funded by Grants-in-Aid for Scientific Research (B) (No. 22300116) and (C) (No. 21500337) from the Japan Society for the Promotion of Science (JSPS) and by the Health and Labor Sciences Research Grants (Research on Measures for Intractable Diseases) from the Ministry of Health, Labor and Welfare of Japan. The authors thank Ms Sachiko Koyama for her technical assistance. The authors also thank Drs Yoshio Tsuboi, Nobutaka Ishizu, Hiroshi Kurisaki and Shigeo Murayama for providing clinical data and pathological materials.

REFERENCES

1. Creutzfeldt HG. On a particular focal disease of the central nervous system (preliminary communication), 1920. *Alzheimer Dis Assoc Disord* 1989; **3**: 3–25.
2. Prusiner SB. Prions. *Proc Natl Acad Sci USA* 1998; **95**: 13363–13383.
3. Doh-Ura K, Iwaki T, Caughey B. Lysosomotropic agents and cysteine protease inhibitors inhibit scrapie-associated prion protein accumulation. *J Virol* 2000; **74**: 4894–4897.
4. Korth C, May BC, Cohen FE, Prusiner SB. Acridine and phenothiazine derivatives as pharmacotherapeutics for prion disease. *Proc Natl Acad Sci USA* 2001; **98**: 9836–9841.
5. Barret A, Tagliavini F, Forloni G *et al.* Evaluation of quinacrine treatment for prion diseases. *J Virol* 2003; **77**: 8462–8469.
6. Collins SJ, Lewis V, Brazier M, Hill AF, Fletcher A, Masters CL. Quinacrine does not prolong survival in a murine Creutzfeldt-Jakob disease model. *Ann Neurol* 2002; **52**: 503–506.
7. Collinge J, Gorham M, Hudson F *et al.* Safety and efficacy of quinacrine in human prion disease (PRION-1 study): a patient-preference trial. *Lancet Neurol* 2009; **8**: 334–344.
8. Caughey B, Brown K, Raymond GJ, Katzenstein GE, Thresher W. Binding of the protease-sensitive form of

PrP (prion protein) to sulfated glycosaminoglycan and congo red [corrected]. *J Virol* 1994; **68**: 2135–2141.
9. Doh-ura K, Ishikawa K, Murakami-Kubo I *et al.* Treatment of transmissible spongiform encephalopathy by intraventricular drug infusion in animal models. *J Virol* 2004; **78**: 4999–5006.
10. Caughey B, Raymond GJ. Sulfated polyanion inhibition of scrapie-associated PrP accumulation in cultured cells. *J Virol* 1993; **67**: 643–650.
11. Shyng SL, Lehmann S, Moulder KL, Harris DA. Sulfated glycans stimulate endocytosis of the cellular isoform of the prion protein, PrPC, in cultured cells. *J Biol Chem* 1995; **270**: 30221–30229.
12. Todd NV, Morrow J, Doh-ura K *et al.* Cerebroventricular infusion of pentosan polysulphate in human variant Creutzfeldt-Jakob disease. *J Infect* 2005; **50**: 394–396.
13. Rainov NG, Tsuboi Y, Krolak-Salmon P, Vighetto A, Doh-Ura K. Experimental treatments for human transmissible spongiform encephalopathies: is there a role for pentosan polysulfate? *Expert Opin Biol Ther* 2007; **7**: 713–726.
14. Tsuboi Y, Doh-Ura K, Yamada T. Continuous intraventricular infusion of pentosan polysulfate: clinical trial against prion diseases. *Neuropathology* 2009; **29**: 632–636.
15. Bone I, Belton L, Walker AS, Darbyshire J. Intraventricular pentosan polysulphate in human prion diseases: an observational study in the UK. *Eur J Neurol* 2008; **15**: 458–464.
16. Caughey B, Lansbury PT. Protofibrils, pores, fibrils, and neurodegeneration: separating the responsible protein aggregates from the innocent bystanders. *Annu Rev Neurosci* 2003; **26**: 267–298.
17. Silveira JR, Raymond GJ, Hughson AG *et al.* The most infectious prion protein particles. *Nature* 2005; **437**: 257–261.
18. Kristiansen M, Deriziotis P, Dimcheff DE *et al.* Disease-associated prion protein oligomers inhibit the 26S proteasome. *Mol Cell* 2007; **26**: 175–188.
19. Minaki H, Sasaki K, Honda H, Iwaki T. Prion protein oligomers in Creutzfeldt-Jakob disease detected by gel-filtration centrifuge columns. *Neuropathology* 2009; **29**: 536–542.
20. Lue LF, Kuo YM, Roher AE *et al.* Soluble amyloid beta peptide concentration as a predictor of synaptic change in Alzheimer's disease. *Am J Pathol* 1999; **155**: 853–862.
21. Sharon R, Bar-Joseph I, Frosch MP, Walsh DM, Hamilton JA, Selkoe DJ. The formation of highly soluble oligomers of alpha-synuclein is regulated by fatty acids and enhanced in Parkinson's disease. *Neuron* 2003; **37**: 583–595.
22. Sasaki K, Minaki H, Iwaki T. Development of oligomeric prion-protein aggregates in a mouse model of prion disease. *J Pathol* 2009; **219**: 123–130.
23. Terada T, Tsuboi Y, Obi T *et al.* Less protease-resistant PrP in a patient with sporadic CJD treated with intraventricular pentosan polysulphate. *Acta Neurol Scand* 2010; **121**: 127–130.
24. Parchi P, Chen SG, Brown P *et al.* Different patterns of truncated prion protein fragments correlate with distinct phenotypes in P102L Gerstmann-Straussler-Scheinker disease. *Proc Natl Acad Sci USA* 1998; **95**: 8322–8327.
25. Kobayashi A, Asano M, Mohri S, Kitamoto T. Cross-sequence transmission of sporadic Creutzfeldt-Jakob disease creates a new prion strain. *J Biol Chem* 2007; **282**: 30022–30028.
26. Cortijo-Arellano M, Ponce J, Durany N, Cladera J. Amyloidogenic properties of the prion protein fragment PrP(185-208): comparison with Alzheimer's peptide Abeta(1-28), influence of heparin and cell toxicity. *Biochem Biophys Res Commun* 2008; **368**: 238–242.

doi:10.1016/j.jmb.2011.08.043 J. Mol. Biol. (2011) 413, 667–683

Contents lists available at www.sciencedirect.com

Journal of Molecular Biology

journal homepage: http://ees.elsevier.com.jmb

Binding and Selectivity of the Marine Toxin Neodysiherbaine A and Its Synthetic Analogues to GluK1 and GluK2 Kainate Receptors

Masaki Unno[1,2,3*], Masanobu Shinohara[2], Koichiro Takayama[2], Hideharu Tanaka[2], Kenta Teruya[4], Katsumi Doh-ura[4], Ryuichi Sakai[5], Makoto Sasaki[6] and Masao Ikeda-Saito[2,3*]

[1]*Frontier Research Center for Applied Atomic Sciences, Ibaraki University, Tokai, Naka, Ibaraki 319-1106, Japan*
[2]*Institute of Multidisciplinary Research for Advanced Materials, Tohoku University, Katahira, Aoba, Sendai 980-8577, Japan*
[3]*RIKEN SPring-8 Center, Harima Institute, Sayo, Hyogo 679-5148, Japan*
[4]*Department of Neurochemistry, Tohoku University Graduate School of Medicine, Seiryo, Aoba, Sendai 980-8575, Japan*
[5]*Graduate School of Fisheries Sciences, Hokkaido University, Hakodate 041-8611, Japan*
[6]*Graduate School of Life Sciences, Tohoku University, Katahira, Aoba, Sendai 980-8577, Japan*

Received 18 April 2011;
received in revised form
11 August 2011;
accepted 23 August 2011
Available online
26 August 2011

Edited by R. Huber

Keywords:
gating efficacy;
discrimination;
ligand;
X-ray structure;
kainate-type ionotropic glutamate receptor

Dysiherbaine (DH) and neodysiherbaine A (NDH) selectively bind and activate two kainate-type ionotropic glutamate receptors, GluK1 and GluK2. The ligand-binding domains of human GluK1 and GluK2 were crystallized as bound forms with a series of DH analogues including DH, NDH, 8-deoxy-NDH, 9-deoxy-NDH and 8,9-dideoxy-NDH (MSVIII-19), isolated from natural sources or prepared by total synthesis. Since the DH analogues exhibit a wide range of binding affinities and agonist efficacies, it follows that the detailed analysis of crystal structure would provide us with a significant opportunity to elucidate structural factors responsible for selective binding and some aspects of gating efficacy. We found that differences in three amino acids (Thr503, Ser706 and Ser726 in GluK1 and Ala487, Asn690 and Thr710 in GluK2) in the ligand-binding pocket generate differences in the binding modes of NDH to GluK1 and GluK2. Furthermore, deletion of the C_9 hydroxy group in NDH alters the ligand conformation such that it is no longer suited for binding to the GluK1 ligand-binding pocket. In GluK2, NDH pushes and rotates the side chain of Asn690 (substituted for Ser706 in GluK1) and disrupts an interdomain hydrogen bond with Glu409. The present data support the idea that receptor selectivities of DH analogues resulted from the differences in the binding modes of the ligands in GluK1/GluK2 and the steric repulsion of

*Corresponding authors. M. Unno is to be contacted at Frontier Research Center for Applied Atomic Sciences, Ibaraki University, 169-1 Shirakata, Tokai, Naka, Ibaraki 319-1106, Japan; M. Ikeda-Saito, Institute of Multidisciplinary Research for Advanced Materials, Tohoku University, Katahira, Aoba, Sendai 980-8577, Japan. E-mail addresses: unno19@mx.ibaraki.ac.jp; mis2@tagen.tohoku.ac.jp.

Present address: K. Teruya, Department of Chemistry, Graduate School of Medical Science, Kyoto Prefectural University of Medicine, Kita-ku, Kyoto 603-8334, Japan.

Abbreviations used: AMPA, α-amino-3-hydroxy-5-methyl-4-isoxazolepropionate; a.u., asymmetric unit; DH, dysiherbaine; EDTA, ethylenediaminetetraacetic acid; iGluR, ionotropic glutamate receptor; KAR, kainate-type ionotropic glutamate receptor; MD, molecular dynamics; MSVIII-19, 8,9-dideoxy-NDH; NDH, neodysiherbaine A; PDB, Protein Data Bank; PEG, polyethylene glycol; s.g., space group.

Asn690 in GluK2. All ligands, regardless of agonist efficacy, induced full domain closure. Consequently, ligand efficacy and domain closure did not directly coincide with DH analogues and the kainate receptors.

Introduction

Ionotropic glutamate receptors (iGluRs) are synaptic receptors that form L-glutamate-gated ion channels and play central roles in excitatory neurotransmission in the mammalian central nervous system. Pharmacologically, iGluRs are classified into three broad subfamilies: *N*-methyl-D-aspartate (NMDA), α-amino-3-hydroxy-5-methyl-4-isoxazole-propionate (AMPA) and kainate-type ionotropic glutamate receptors (KARs).[1,2] The iGluR subfamily is composed of a total of 18 proteins. Isoforms within each subfamily assemble into homomeric or heteromeric oligomers in certain combination in order to form functional ion channels. Thus, functional synaptic receptors are highly diverse and inherently difficult to characterize.

Naturally occurring toxins represent valuable tools for neuropharmacological research, as they often selectively target neuronal receptors with high affinity, and they are able to modulate receptor function in unexpected ways. Dysiherbaine (DH) and neodysiherbaine A (NDH), isolated from the marine sponge *Lendenfeldia chondrodes*, provide a particularly interesting example of such a molecule. DH and NDH have been shown to be potent convulsants in mice and have been characterized as potent agonists for KARs.[3–5] DH has also been shown to bind selectively and to have unusually high affinity for both GluK1 (formerly known as GluR5) and GluK2 (GluR6) KAR isoforms and can selectively activate subunits in some heteromeric receptor complexes.[4,6] Thus, DH, NDH and their analogues may serve as interesting tools that characterize neuronal KARs in detail.[7–10]

Exploration of the structure–function relationships related to the function of DH analogues has yielded interesting and unexpected aspects of GluK1 and GluK2 KARs.[9,11,12] Structurally, DH and NDH contain a shared template, consisting of a *cis*-fused hexahydrofuro[3,2-*b*]pyran ring system with two functional groups at the C_8 and C_9 positions, in addition to a glutamate substructure (Fig. 1). Since relatively small differences in the functional groups at C_8 were found to impart significant effects upon binding affinity and selectivity as revealed by comparing the activity of DH and NDH, a series of NDH analogues including 8-deoxy-NDH, 9-deoxy-NDH and 8,9-dideoxy-NDH (MSVIII-19) was synthesized.[7,13] The binding affinities of these compounds for GluK1 and GluK2 are summarized in Table 1. For example, DH and NDH also bind strongly to GluK2, although 8-deoxy-NDH has a much lower affinity for GluK2 than those of DH and NDH. Furthermore, 9-deoxy-NDH and MSVIII-19 do not bind to GluK2.[11] These binding profiles are rather unexpected considering the structural similarity of both ligands and receptors, where GluK1 and GluK2 have 74% and 87% identity overall in terms of ligand-binding-core sequence identity, respectively.[15] Several functional aspects of the DH analogues are also intriguing. For example, it has been shown that DH, NDH and 8-deoxy-NDH are full or efficient agonists for GluK1, while 9-deoxy-NDH is only a partial agonist.[11] Moreover and of most interest is that MSVIII-19 acts as a

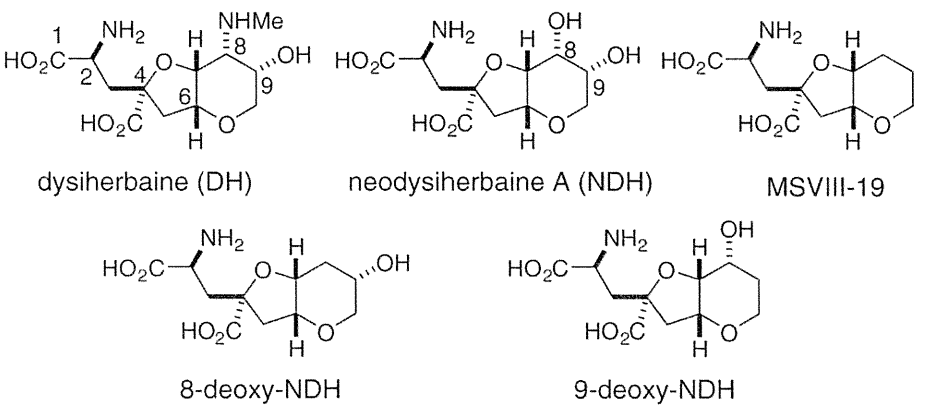

Fig. 1. Chemical structures of DH and its analogues.

Table 1. K_i values for displacement of [^{3}H]kainate by DH analogues[4,11,12,14]

K_i (nM)	L-glutamate	DH	NDH	MSVIII-19	8-deoxy-NDH	9-deoxy-NDH
GluK1	290	0.5	7.7	128	1.5	169
GluK2	1080	1.3	33	>100,000	48,000	>100,000

potential antagonist for GluK1.[12] Furthermore, MSVIII-19 induced a coma-like sleeping state in mice when administrated intracerebroventricularly, rather than induce convulsions. Recently, MSVIII-19 was also shown to exert analgesic properties in mice when applied intrathecally.[16] Collectively, these data indicated that although the structure–function relationships of DH analogues are complex, the polar functional groups at C_8 and C_9 play intriguing roles in the binding and gating of KARs. Recently, the crystal structures of rat GluK1 ligand-binding core (GluK1-S1S2) in complex with DH and MSVIII-19 were elucidated.[17] The structures showed that MSVIII-19 induced a full domain closure of GluK1-S1S2 instead of an "open" structure for the receptor in complex with an antagonist.[17] These results were contradictory to the previous proposal that antagonists stabilize an "open" rather than "closed" state of the receptor–ligand complex.[18–20] Accordingly, the gating properties of MSVIII-19 were further characterized at the pharmacological level and shown to induce gating current in only a very poor manner but desensitized the receptor effectively, thus acting as a functional antagonist.[16,17] It was thus concluded that, with GluK1, gating efficacy was not necessarily related to an agonist's ability to "close" the ligand-binding domain.[17]

These drastic changes in the mode of activity and isoform selectivity as a result of only a relatively small change in the functional group observed in NDH analogues are intriguing issues to explore further. Detailed analyses of the crystal structures of GluK1-S1S2 in complex with various NDH analogues with a wide range of binding affinities and agonist efficacies would further elucidate some of these interesting observations. Since we have developed a synthetic route that enables a relatively large supply of a series of DH analogues,[7,8,10] we conducted the crystallization of the human GluK1-S1S2 (hGluK1-S1S2) in complex with DH, NDH, MSVIII-19, 8-deoxy-NDH and 9-deoxy-NDH and obtained the structures at 1.5 Å resolution. In addition, we also obtained the structure of the hGluK1-S1S2 complex with L-glutamate at 1.65 Å resolution (Supporting Information, Table S1 and Fig. S1). Finally, we determined the crystal structure of the human GluK2-S1S2 (hGluK2-S1S2) in complex with NDH (Supporting Information and Table S1). In this paper, we describe detailed structures of the receptor–ligand complex, present a comparative view of structural implication in light of both receptor and ligand conformations and discuss differences in binding patterns arising from the structural alteration of the molecule.

Results

Overall structure

Amino acids are numbered with respect to mature proteins in accordance with the recommendations by Mayer,[21] and the corresponding residue numbers of preprocessed forms[17,22] are shown in parentheses.

The hGluK1-S1S2 crystals obtained during this study belonged to two different types of space groups (s.g.s): *C*2 and *P*1 (Supporting Information and Table S1). We obtained *P*1 crystals with high reproducibility in complex with L-glutamate, DH, NDH, MSVIII-19, 8-deoxy-NDH or 9-deoxy-NDH at up to 1.5 Å resolution (1.65 Å for L-glutamate) (Supporting Information and Fig. S1). However, *C*2 crystals were obtained for only the L-glutamate, DH and NDH complexes with very poor reproducibility. It is possible that the protein structures in *C*2 crystals may be an artifact (see Supporting Information for details). Comparisons of *P*1 and *C*2 crystals are also described in Supporting Information. We thus utilized molecules from *P*1 crystals as hGluK1-S1S2 throughout the discussion.

The hGluK1-S1S2 monomer has two subdomains, namely, domain 1 [residues 420–520 (435–535) and residues 747–786 (762–801)] and domain 2 [residues 521–746 (536–761)], as depicted in Fig. 2a. Each ligand was located between domain 1 and domain 2. The overall structures of hGluK1-S1S2s monomers are essentially the same, irrespective of bound ligands [C^α root-mean-square (r.m.s.) differences are 0.1–0.40 Å]. The monomer of hGluK1-S1S2 interacts with the other monomer in a dominant manner via domain 1 (Fig. 2b). The intermolecular varied area was 7226 Å^2. One monomer can be generated by reflecting a plane and rotating approximately 80° against the other monomer (Fig. 2b). The structures of the two monomers are essentially the same with a C^α r.m.s. difference of 0.35 Å.

Crystals of hGluK2-S1S2 were obtained in complex with NDH, belonging to s.g. $P2_1$, and contained two molecules in its asymmetric unit (a.u.). Structure was determined at 1.65 Å resolution (Supporting Information and Table S1). The monomer structure was similar to that of the hGluK1-S1S2–NDH

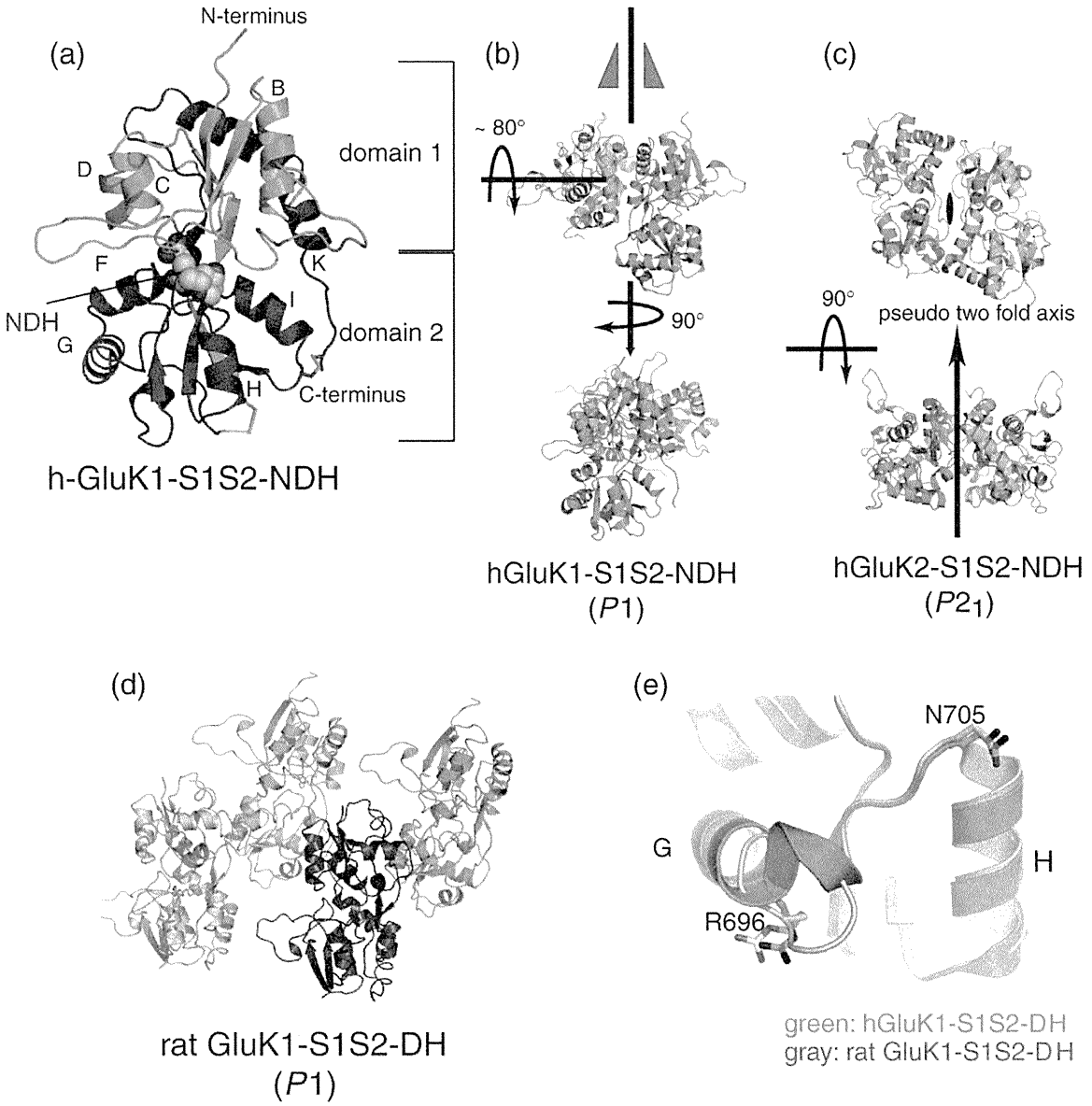

Fig. 2. The overall structure of hGluK1-S1S2 in complex with NDH. (a) S1 and S2 segments are shown in green and magenta, respectively. NDH is depicted by the CPK model (C, N and O atoms are represented as yellow, blue and red, respectively). Initials represent α-helices, which are named in accordance with Mayer's recommendations.[21] (b) hGluK1-S1S2 monomer–monomer interaction in *P*1 crystals and (c) monomer–monomer interaction in hGluK2-S1S2, viewed from two directions. Monomers are depicted in green and cyan. (d) Four molecules of rat GluK1-S1S2 in the a.u. Monomers are depicted in green, cyan, magenta and yellow. Intermolecular interactions are quite different from those in human. (e) Superposition of hGluK1-S1S2 (green) and rat GluK1-S1S2 (gray).

complex with a C^{α} r.m.s. difference of 0.85 Å and was essentially the same as that of the rat GluK2-S1S2 L-glutamate complex reported previously[21] with a C^{α} r.m.s. difference of 0.60 Å.

The hGluK2-S1S2 monomer interacts with the other monomer in a head-to-tail fashion (Fig. 2c). The intermolecular interaction is quite different from that found in the hGluK1-S1S2 in the *P*1 crystals. The intermolecular varied area was 6893 $Å^2$. One monomer can be generated by rotation against a pseudo-2-fold axis (Fig. 2c). The C^{α} r.m.s. difference between the two monomers was 0.29 Å.

The clear differences in the dimer structure between hGluK1-S1S2 and hGluK2-S1S2 imply that the ligand-binding core of KARs should be considered as a monomer, as highlighted by Frydenvang *et al.*[17]

Comparative structural analysis with reference to DH and MSVIII-19 complex structures reported previously

Frydenvang *et al.* previously reported crystal structures for rat GluK1-S1S2 in complex with DH and MSVIII-19.[17] Since three residues, Leu463 (478), Ser700 (715) and Lys704 (719) and Ile463 (478), Thr700 (715) and Arg704 (719), in the ligand-binding core of rat and human, respectively, are different and since the crystallization conditions employed were not identical between existing studies, we decided

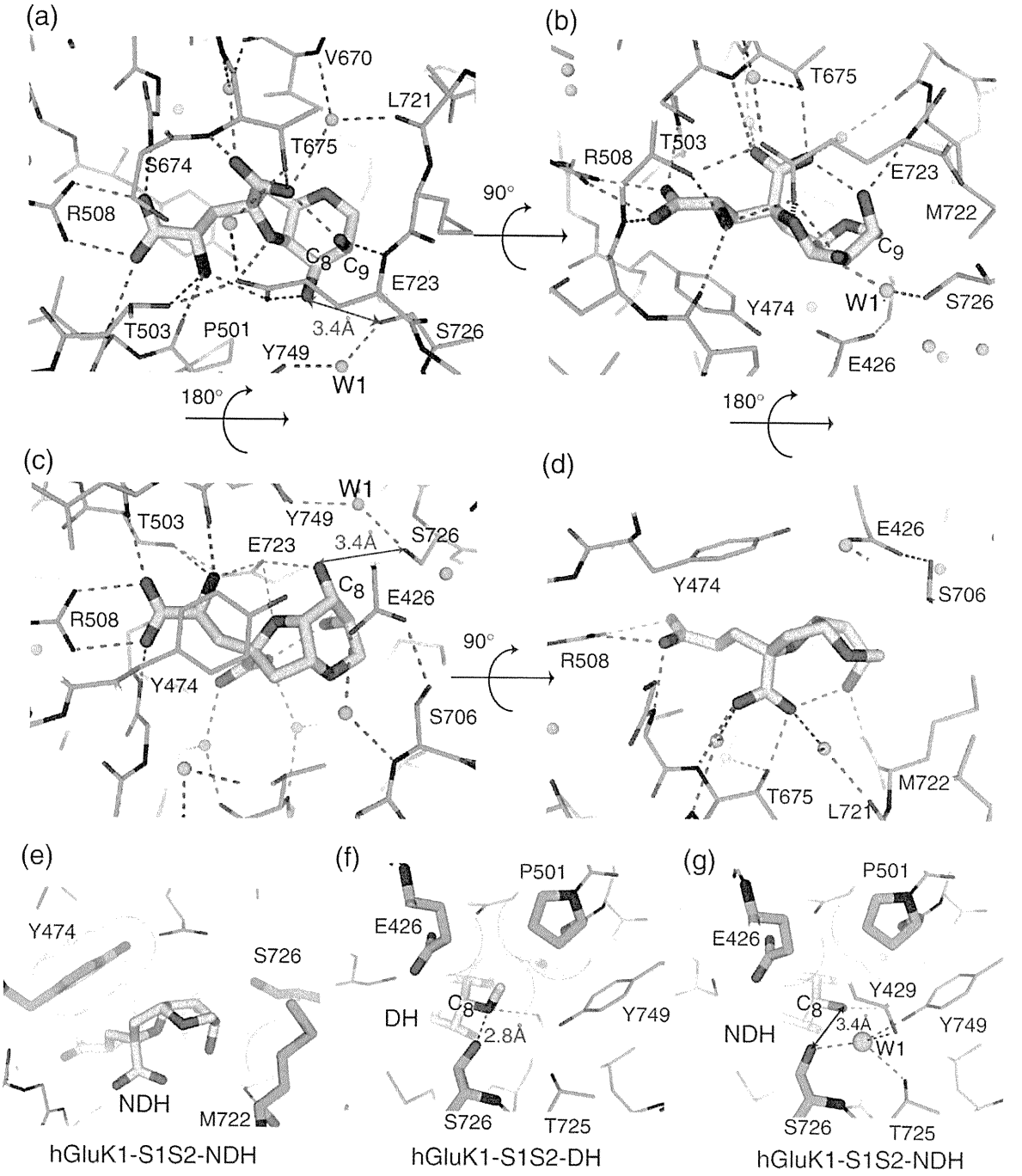

Fig. 3. Modes of ligand binding in hGluK1-S1S2. (a–d) Hydrogen-bonding interactions between NDH and surrounding residues from four directions. Cyan balls represent water molecules. (e) van der Waals contacts between NDH and GluK1 ligand-binding domain. (f) van der Waals contacts and hydrogen-bonding interactions between the DH *N*-methylamino group and GluK1. (g) van der Waals contacts in the hGluK1-S1S2–NDH complex. The cyan ball indicates the nearby water molecule, which is found only in the NDH complex.

Table 2. Hydrogen-bonding interactions between NDH and hGluK1-S1S2 and between NDH and hGluK2-S1S2 (average distances of two molecules in the a.u.)

NDH	hGluK1-S1S2	Average distance (Å)	hGluK2-S1S2	Average distance (Å)
C_8OH	Glu723O$^{\varepsilon 1}$	2.79	Glu707O$^{\varepsilon 1}$	2.91
C_8OH	—	—	Thr710OH	2.66
C_9OH	Glu723N	2.78	Glu707N	2.78
Five-membered ring O	Glu723O$^{\varepsilon 1}$	3.04	Glu707O$^{\varepsilon 1}$	3.18
Six-membered ring O	—	—	Water 1	3.14
Glutamate O1	Thr503N	2.85	Ala488N	2.87
Glutamate O1	Arg508N$^{\eta 1}$	2.83	Arg493N$^{\eta 1}$	2.86
Glutamate O2	Arg508N$^{\eta 2}$	2.77	Arg493N$^{\eta 2}$	2.71
Glutamate O2	Ser674N	2.78	Ala658N	2.79
Glutamate N	Thr503OH	2.92	—	—
Glutamate N	Glu723O$^{\varepsilon 1}$	2.83	Glu707O$^{\varepsilon 1}$	2.76
Glutamate N	Pro501O	2.86	Pro486O	2.85
Glutamate γ-carboxylate OAA	Thr675OH	2.67	Thr659OH	2.60
Glutamate γ-carboxylate OAA	Water 1	3.19	—	—
Glutamate γ-carboxylate OAE	Thr675N	3.05	Thr659N	3.03
Glutamate γ-carboxylate OAE	Water 2	2.86	Water 2	2.67

first to carry out a detailed analysis of the structure. Crystals of rat GluK1-S1S2 in complex with DH belonged to s.g. *P*1 and contained four monomers in the a.u.,[17] whereas the human counterpart contained just two monomers (Fig. 2b and d). Overall, the monomer structures of rat and human DH complexes were quite similar, except for a few residues in the N-terminal region and some flexible loops. The overall C$^{\alpha}$ r.m.s. difference was 0.99 Å. DH-binding regions were similar. We identified two conformations of the Tyr429 (444) side chain in our present structure, while only a single conformation was observed in the rat counterpart (Supporting Information and Fig. S3). However, the importance of these Tyr429 (444) conformations remains unclear. The largest differences in structure were detected in the loop conformation between helix G and helix H [between Arg696 (711) and Asn705 (720)] (Fig. 2e). Only these two points can be considered as salient differences between the two structures. All other structural aspects remain almost identical. The DH-binding mode remained essentially the same.

The crystal of hGluK1-S1S2 in complex with MSVIII-19 belonged to s.g. *P*1 and contained two monomers in the a.u. as reported previously for the rat MSVIII-19 complex.[17] Overall, monomer structures of human and rat MSVIII-19 complexes were similar apart from a flexible loop between Arg696 (711) and Asn705 (720). The overall C$^{\alpha}$ r.m.s. difference was 1.01 Å. Thus, the structures of MSVIII-19-binding regions and its binding mode in human and rat receptors can be considered to be essentially the same (*vide infra*). The Tyr429 (444) side chain exhibited a single conformation.

Binding mode of NDH in hGluK1-S1S2

NDH was shown to bind to the ligand-binding pocket of hGluK1-S1S2 in a manner similar to that observed with DH. The bulky bicyclic portion of the ligand expelled four water molecules originally found in the L-glutamate complex,[21,22] enabling direct hydrogen-bonding interaction with the protein (Fig. 3a–d and Table 2). van der Waals interactions between the C_5, C_7 and C_8 atoms in the bicyclic portion with Tyr474 (489), Met722 (737)C$^{\gamma}$ or Ser726 (741)C$^{\beta}$ were also present in the NDH complex, in which the C–C distance was between 3.4 and 4.1 Å (Fig. 3e).

The role of C_8 functional groups in the GluK1-S1S2 ligand-binding pocket

As previously reported, in the DH complex, the C_8 *N*-methylamino group engaged in van der Waals interactions with Glu426 (441)C$^{\gamma}$, Pro501 (516)C$^{\beta}$ and Pro501 (516)C$^{\gamma}$ (Fig. 3f).[17] In addition, hydrogen-bonding interactions were formed between the C_8 *N*-methylamino group and Ser726 (741)OH (Fig. 3f). Molecular dynamics

Fig. 4. Differences in the three-dimensional structure between 9-deoxy-NDH and NDH bound to hGluK1-S1S2. (a) The structure of NDH; (b) the structure of 9-deoxy-NDH. (c) Modeled 9-deoxy-NDH fitting the $F_o - F_c$ electron density map contoured at 3.0-σ level calculated without 9-deoxy-NDH viewed from two directions. (d) 9-Deoxy-NDH shows loss of van der Waals contacts with Glu426 (441). (e) Superposition of 9-deoxy-NDH (yellow-based) and MSVIII-19 (gray-based). Numbers written in magenta represent carbon atoms in 9-deoxy-NDH, while those written in black are carbon atoms in MSVIII-19. (f) 9-Deoxy-NDH shows double conformations, predominantly in a twisted-boat form but also partly in an extended chair form. Vivid yellow represents the major conformation in a twisted-boat form, which is refined with occupancy at 0.6. Lime and pink represent the minor conformation in a chair form, which is refined with occupancy at 0.4. The latter is very similar to the structure of MSVIII-19. The main chain is modeled in single conformation.

(MD) simulation results suggested that hydrogen bonding may represent a key factor underlying the pharmacological specificity of DH.[23] Furthermore, the C_8 *N*-methylamino group of DH is stabilized by hydrogen-bonding interactions with Glu723 (738) carboxylate. All such interactions

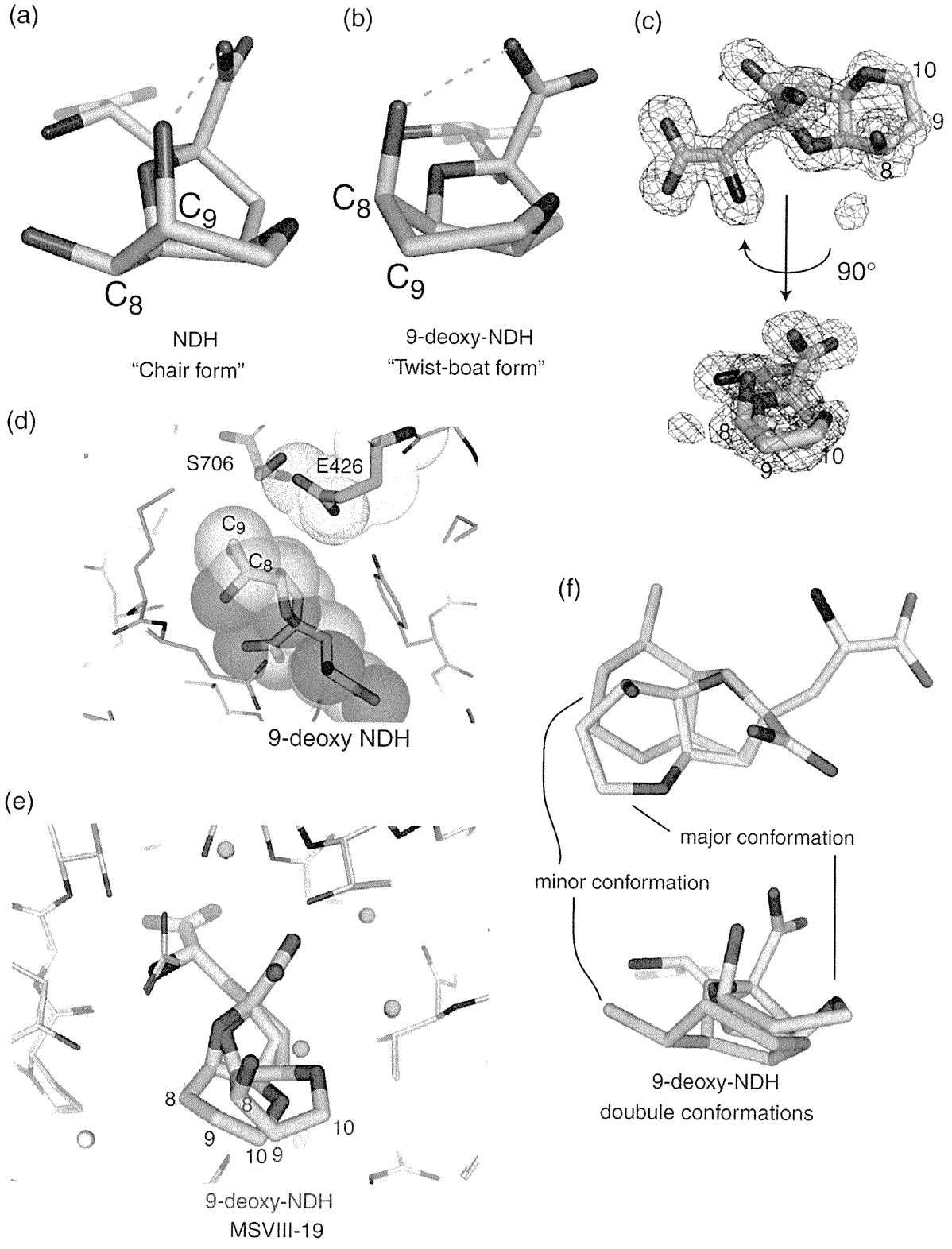

Fig. 4 (*legend on previous page*)

were reproduced in the hGluK1-S1S2–DH complex (Fig. 3f).

In the case of NDH, the conformations of both ligand and the surrounding residues might change slightly, compared to those of the DH complex. This is due to the differences in the C_8 functional groups when DH and NDH are compared. In the NDH complex, we observed that the distance between the C_8 hydroxy group and Ser726 (741)OH was 3.4 Å, which is too far to allow effective hydrogen-bonding interaction (Fig. 3a, c and g). A lack of a methyl group at the oxygen atom at C_8 in NDH excludes the stabilizing effect of van der Waals interactions (Fig. 3g), which were observed in the DH complex (Fig. 3f). Thus, the difference in the C_8 functionality may explain the lower affinity of NDH for GluK1 as compared to that of DH (Table 1).

In addition, we observed a water molecule (W1) that intervenes between the C_8 hydroxy group and the protein matrix in the NDH complex (Fig. 3). This water molecule was stabilized by Tyr429 (444)OH, Thr725 (740)OH, Ser726 (741)OH and Tyr749 (764) OH with hydrogen bonds (Fig. 3g). Although interatomic distance between the C_8 hydroxy group of NDH and W1 (3.0 Å) may allow the formation of hydrogen bonds, its contribution in stabilizing the complex is likely to be negligible since the affinity of 8-deoxy-NDH for GluK1 is comparable with that of NDH (Table 1). Of particular note, W1 was indeed found in the structure of the 8-deoxy-NDH complex (Supporting Information and Fig. S1) as well but not in the DH complex (Fig. 3f).

Importance of the C_9 hydroxy group in NDH analogues for the protein–ligand complex stability

In the crystal structures of DH, NDH and 8-deoxy-NDH bound to hGluK1-S1S2, distances between the C_9 hydroxy group and the γ-carboxylate within the glutamate substructure were within 2.9 Å, suggesting the presence of hydrogen-bonding interaction between them (Fig. 4a). This peculiar intramolecular interaction resulted in these ligand molecules exhibiting highly folded conformations. In contrast, MSVIII-19 did not exhibit such interactions since it lacked a C_9 hydroxy group, as reported previously.[17] Unexpectedly, however, we found that a major conformer of 9-deoxy-NDH in complex with GluK1 formed an intramolecular hydrogen bond between its C_8 hydroxy group and the γ-carboxylate of the glutamate substructure, rather than the C_9 hydroxy group. Consequently, the tetrahydropyran ring of 9-deoxy-NDH predominantly exists in a twisted-boat form (Fig. 4b and c). Owing to this distorted boat conformation, the van der Waals interaction between the tetrahydropyran ring and Glu426 (441)C^{δ} is lost (Fig. 4d). The C_9 atom of 9-deoxy-NDH is positioned at almost the same point as the C_{10} atom of MSVIII-19 when superimposed (Fig. 4e). Interestingly, a minor conformer that lacks a hydrogen bond with the γ-carboxylate was also found in the electron density map (Fig. 4c and f). Collectively, these results indicated that the C_9 hydroxy group of NDH analogues represents a key functional group not only for forming hydrogen-bonding interaction with Glu723 (738) main-chain amide (Fig. 3a and b) but also for maintaining the unique conformation by the intramolecular hydrogen bond with the γ-carboxylate (Fig. 4a).

Differences in NDH-binding modes in GluK1 and GluK2

Ligand-binding-core structures of human GluK1 and GluK2 are very similar and share 87% sequence identity. However, GluK1 possesses a binding cavity larger than that of GluK2,[21] and ligand binding to GluK2 is generally less favorable than that to GluK1.[21,24] As Lash *et al.* have reported previously, GluK1/GluK2 selectivity differs significantly among the NDH analogues, although the size of these molecules does not differ drastically.[11] Thus, the crystal structures obtained in this study for the NDH complex with GluK2 are likely to provide us with significant insight into the associated binding properties.

The crystal structures of NDH complexes with GluK1 and GluK2 were similar, but intriguing differences in some binding profiles were observed between NDH-bound GluK1 and GluK2. These differences were analogous to the L-glutamate-bound structures of GluK1 and GluK2.[21] Thr503 (518) in GluK1 formed two hydrogen bonds between the α-amino group of NDH and the δ-carboxylate of Glu723 (738) (Fig. 5a), whereas a lack of direct hydrogen bonding with the corresponding residue Ala487 (518) in GluK2 resulted in a slight change in conformation and orientation at Glu707 (738) (Fig. 5b). The C^{α}–C^{β} axis of Glu707 (738) in GluK2 was tilted by ~10° compared to that of Glu723 (738) in GluK1. The orientation and conformation of NDH were also different in both receptors. The glutamate substructure of NDH was tilted by 5°, and the bulky bicyclic portion of NDH in GluK2 was rotated about 10° around the C_3–C_4 axis. These differences induced a shift in their positions by approximately 1.0 Å (Fig. 5c).

In GluK1, a water molecule (W1) was found in close proximity to the C_8 hydroxy group of NDH. The distance between Ser726 (741)OH and the C_8 hydroxy group was 3.4 Å (Figs. 3a and c and 5a). These data suggest that a direct hydrogen bond between the C_8 hydroxy group of NDH and Ser726 (741)OH in GluK1 is not effective (*vide supra*). However, in the case of GluK2, Thr710 (741), which corresponds to Ser726 (741) in GluK1, can form direct hydrogen bonds with the C_8 hydroxy group

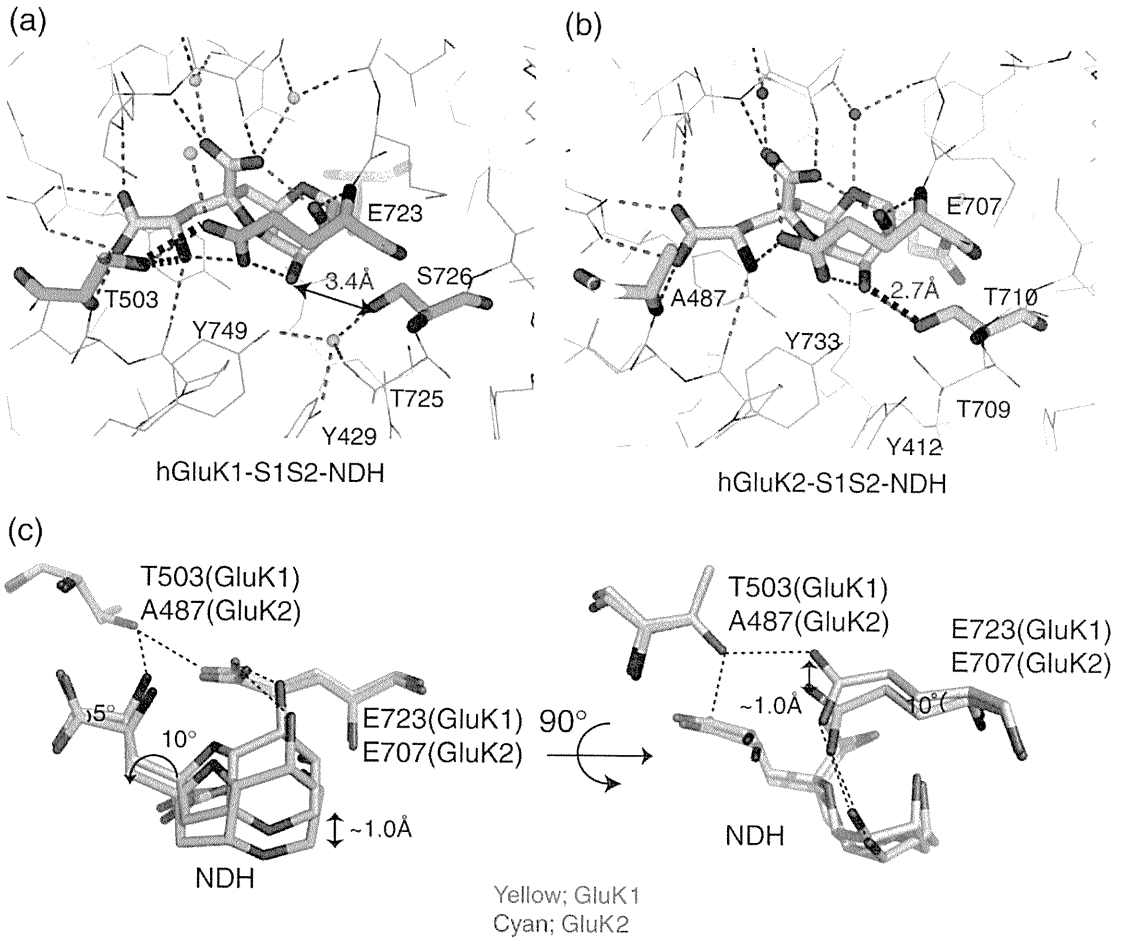

Fig. 5. Differences in the modes of NDH binding in GluK1 and GluK2. (a) NDH in GluK1. (b) NDH in GluK2. (c) Structural displacement of NDH and the nearby glutamate. The yellow-based figure is in GluK1, and the cyan-based figure is in GluK2. Pictures from the two point of views are depicted in order to clarify the conformation and orientation changes in NDH and the nearby glutamate.

of NDH, a feature attributable to their closer proximity (2.7 Å) (Fig. 5b). Moreover, the proximity between other proton donors and acceptors within the bicyclic portion of NDH and the protein matrix in GluK1 and GluK2 is different (summarized in Table 2). Consequently, the hydrogen-bonding network formed between NDH and GluK1 or GluK2 might be one of the factors that differentiate the binding affinity of NDH to the receptors (see Discussion).

Conformation of Asn690 in GluK2

The most significant difference identified in the structure of the hGluK2-S1S2–NDH complex, when compared to the L-glutamate complex [Protein Data Bank (PDB) ID 1S50][21] or the kainate complex (PDB ID 1TT1)[21] of GluK2, was the conformation of Asn690 (721). In the structure of rat GluK2-S1S2 in complex with L-glutamate or kainate, the side chain of Asn690 (721) points toward the bound ligands (Fig. 6a and b). In contrast, in the NDH complex, Asn690 (721) points away from the ligand due to steric hindrance between the side chain and the six-membered ring of NDH (Fig. 6c). This rather drastic conformational change in Asn690 (721) resulted in disruption of the hydrogen bond between Glu409 (441) and Asn690 (721). The distance between Glu409 (441)$O^{\varepsilon 2}$ and Asn690 (721)$N^{\delta 2}$ was 3.9 Å, and the angle Glu409 (441)$O^{\varepsilon 2}$–Asn690 (721)$N^{\delta 2}$–Asn690 (721)C^{γ} was 75°, which is too far and too acute to form hydrogen bonds. These data suggest that NDH binding forced rotation of the Asn690 side chain, which is not required in smaller ligands such as L-glutamate and kainate (Fig. 6a and b). The corresponding Ser706 (721) conformation in hGluK1-S1S2–NDH did not differ from that seen in the L-glutamate complex of GluK1 because serine is smaller than asparagine [Asn690 (721) in GluK2], and thus, NDH can bind to the GluK1 ligand-binding pocket without conformational change (Fig. 6d).

Glu409 (441) and Asn690 (721) are located at the entrance of the ligand-binding cleft in GluK2 (Fig. 6e). Breakage of the hydrogen bond between them was discovered even when an efficacious agonist NDH was bound to GluK2 in this study.

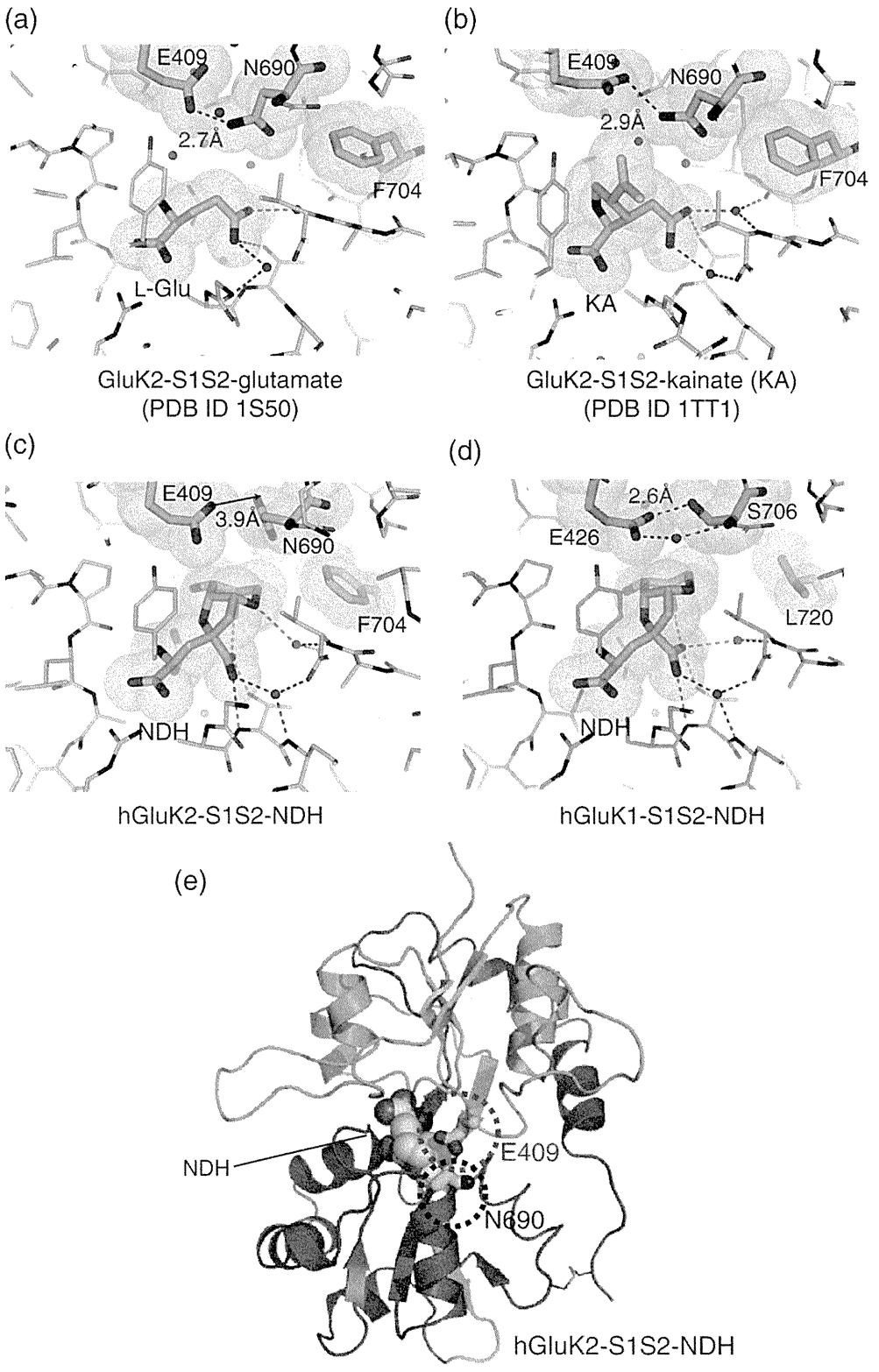

Fig. 6 (*legend on next page*)

Table 3. Distance measurements between domain 1 and domain 2 of hGluK1-S1S2

		Distances (Å)			
		Ser706C$^{\alpha}$–Glu426C$^{\alpha}$	Glu723C$^{\alpha}$–Pro501O	Asp672O–Gly475N	Ser674C$^{\alpha}$–Thr503C$^{\alpha}$
L-glutamate	Molecule A	7.46	8.87	2.89	6.54
	Molecule B	7.24	8.83	2.91	6.54
	Average	7.35	8.85	2.90	6.54
DH	Molecule A	7.55	8.88	2.88	6.49
	Molecule B	7.34	8.93	2.88	6.50
	Average	7.45	8.91	2.88	6.50
NDH	Molecule A	7.52	8.84	2.86	6.53
	Molecule B	7.63	8.87	2.89	6.52
	Average	7.58	8.86	2.87	6.53
MSVIII-19	Molecule A	7.66	8.69	2.89	6.61
	Molecule B	7.60	8.69	2.86	6.58
	Average	7.63	8.69	2.88	6.60
8-deoxy-NDH	Molecule A	7.60	8.74	2.87	6.54
	Molecule B	7.52	8.75	2.86	6.57
	Average	7.56	8.75	2.87	6.56
9-deoxy-NDH	Molecule A	7.61	8.82	2.87	6.58
	Molecule B	7.48	8.79	2.85	6.58
	Average	7.55	8.81	2.86	6.59

Residue pairs were selected in accordance with those in Ref. 26.

Domain closure of hGluK1-S1S2 upon ligand binding

As demonstrated previously for rat GluK1-S1S2,[17] hGluK1-S1S2 showed the induction of full domain closure for DH, NDH and their synthetic analogues. No domain motions were identified by DynDom[25] when compared to the structure of the L-glutamate complex obtained under similar crystallization conditions. Distances between the centers of masses for domains 1 and 2 were very similar (23.82, 23.65, 23.76, 23.92, 23.82 and 23.85 Å for L-glutamate, DH, NDH, MSVIII-19, 8-deoxy-NDH and 9-deoxy-NDH complexes, respectively). In order to compare the previous MD simulation by Postila *et al.*,[26] we also measured the distances between selected atom pairs reflecting to cleft opening (Table 3). In the crystal structures, none of the ligands induced cleft opening. Hydrogen-bonding interactions between Asp672 (687)N and Gly475 (490)O and the side chains of Glu426 (441) and Ser706 (721)[26] were maintained in all structures.

In the previous study, DH, NDH and 8-deoxy-NDH were characterized as full or relatively efficacious agonists for GluK1, and 9-deoxy-NDH was shown to be a partial agonist with low efficacy, while MSVIII-19 was a potential antagonist.[11,12,16,23] Thus, the present results clearly indicate that, in DH analogues, induction of domain closure does not correlate directly with their agonist efficacy for GluK1 as has been suggested earlier by Frydenvang *et al.*[17]

Since the "twist" motion of the bottom lobe relative to the upper lobe of the ligand-binding core was recently proposed as being one of the factors that affect agonist efficacy in the AMPA receptors,[27] we compared the structures of the L-glutamate complex and a series of DH analogue complexes. At first, we superposed each ligand complex structure to the L-glutamate complex. Then we determined the principal axis and the vertical axis as described in a structural study for AMPA receptors (Fig. 7a). Vector from the center of mass of domain 2 to that of domain 1 was calculated for each ligand complex, then the L-glutamate complex vector was subtracted from the ligand complex vector (Fig. 7b). The twist motion between the two domains would be indicated by offset from the center in the graph. However, the maximum displacement was 0.3 Å; this value was not significantly larger compared to the crystallographic error range at 1.5 Å resolution.

Fig. 6. Conformations of Asn690 (721) in GluK2 and the corresponding residue Ser706 (721) in GluK1. (a) GluK2-S1S2–L-glutamate complex (PDB ID 1S50), (b) GluK2-S1S2–kainate complex (PDB ID 1TT1) and (c) hGluK2-S1S2–NDH complex. In the NDH complex, Asn690 (721) is toward the opposite side of the bound ligand only in the NDH complex. Asn690 (721) formed a hydrogen bond to Glu409 (441) in the L-glutamate and the KA complex, but the hydrogen bond was disrupted in the NDH complex. (d) hGluK1-S1S2–NDH complex. Residues Glu409 (441), Asn690 (721) and Phe704 (735) in GluK2; Glu426 (441), Asn706 (721) and Leu720 (735) in GluK1; and ligands have been encircled by a transparent van der Waals sphere. (e) Overall structure of hGluK2-S1S2 and positions of Glu409 (441) and Asn690 (721). S1 and S2 segments are represented as green and magenta, respectively. NDH is depicted by the CPK model (C, N and O atoms are represented as yellow, blue and red, respectively). Glu409 (441) and Asn690 (721) are highlighted with stick representation (cyan-based).

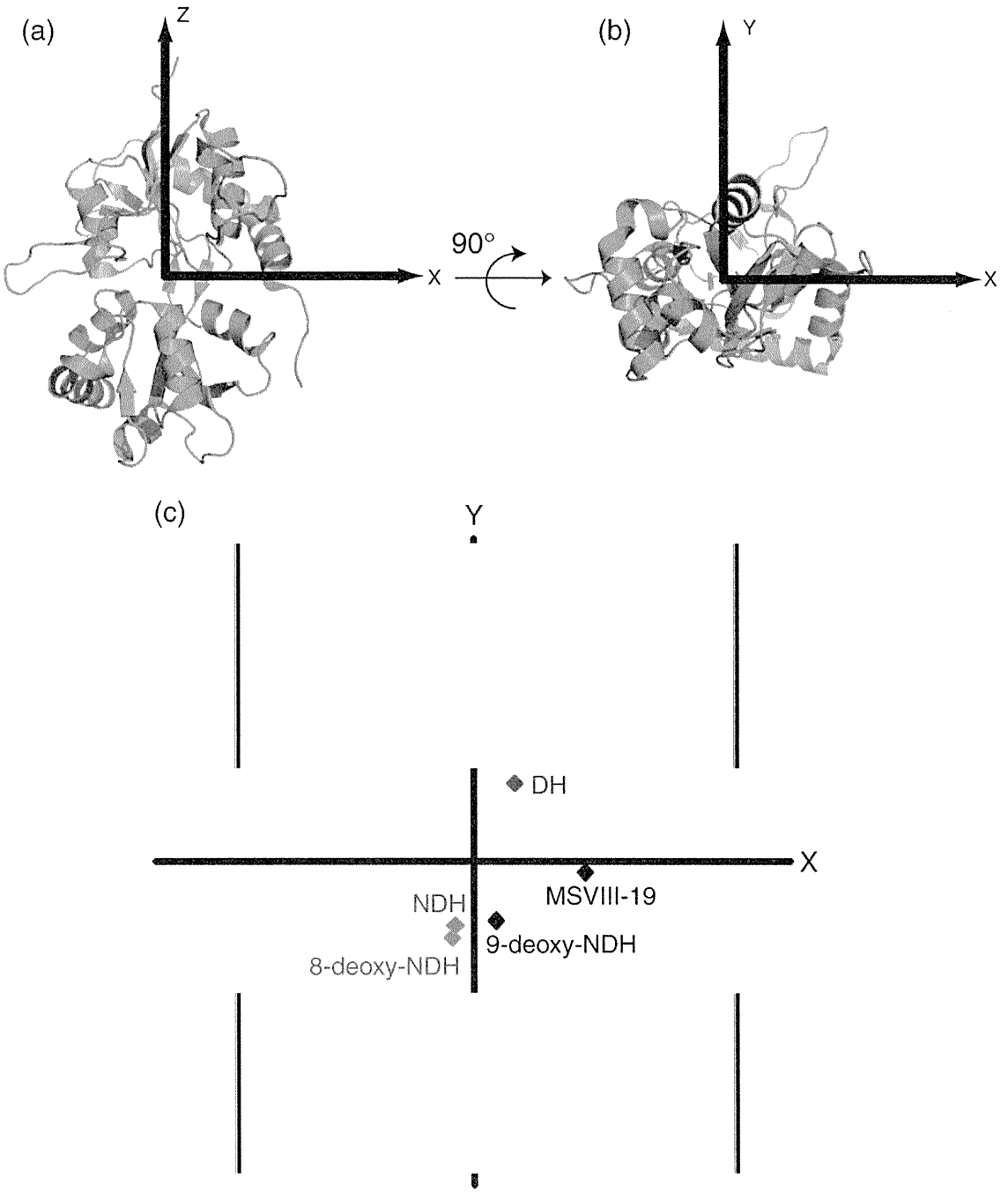

Fig. 7. Principle-axis analysis does not show significant conformational responses of hGluK1-S1S2 in binding ligands. (a and b) The structure of hGluK1-S1S2 was aligned to its principal axes as shown in face (a) and bottom (b) views of the domain. (c) To visualize twist motion associated with ligand binding, we show the center-of-mass displacements of domain 2. Colored marks represent the end points of vectors from the center of mass of domain 2 to the center of mass of domain 1 of the ligand complex subtracted by the corresponding vectors for the L-glutamate complex. Red, DH; orange, NDH; blue, MSVIII-19; green, 8-deoxy-NDH; purple, 9-deoxy-NDH.

Discussion

DH and NDH are naturally occurring amino acids that bind strongly to GluK1 and GluK2. Their synthetic analogues, 8-deoxy-NDH, 9-deoxy-NDH and MSVIII-19, exhibit a wide range of binding potency and agonist efficacy (Table 1). In the present study, we determined the structures of hGluK1-S1S2 in complex with six different ligands: L-glutamate, DH, NDH, MSVIII-19, 8-deoxy-NDH

and 9-deoxy-NDH. We also determined the structure of hGluK2-S1S2 in complex with NDH. The structures of rat GluK1-S1S2 complexed with L-glutamate, DH and MSVIII-19 and the structure of rat GluK2-S1S2 complexed with L-glutamate have been reported previously.[17,21,22] Results generated during the present study provided us with an opportunity to investigate the structural basis of binding and function in important agonists, DH analogues, for GluK1 and GluK2.

The first and most obvious question to consider was whether observed differences between rat and human receptors reflect any structural changes within agonist–receptor complexes, as the only difference between these receptors is a three-amino-acid sequence in the ligand-binding core (Supporting Information and Fig. S4; UniProtKB P22756 and P39086 for rat and human sequences, respectively). As expected, our present results confirmed the close similarity in structure and ligand-binding mode between the human and the rat receptor–ligand complexes. However, we also observed several differences including loop orientation between helices G and H, where 2 out of 10 amino acids differ between human and rat (Fig. 2e). We also noted two different conformations for Tyr429 (444) in the human DH complex, although no such variation has been reported for the other complexes. However, the physiological importance of these differences remains unclear.

Our data provided several interesting implications for binding mode between DH analogues and GluK1 and GluK2. Previous results indicated that removal of the C_8 hydroxy group of NDH drastically reduced affinity for GluK2 while maintaining affinity for GluK1. Furthermore, deletion of the C_9 hydroxy group prevents ligands from binding to GluK2. Such properties are fundamental to the binding selectivity of the ligands for GluK1 and GluK2 (Table 1).[11] These data raised the question of why apparently smaller analogues lose affinity to GluK2, even though the volume of the binding pocket for GluK2 was smaller than that of GluK1?[21] This point has been discussed previously by Lash *et al.* on the basis of MD simulation.[11] Since the present study provides the first experimental evidence to show atomic interactions between GluK2 and NDH, we had the opportunity to address general aspects of binding mode. As proposed earlier, the C_8 and C_9 hydroxy groups are important in that they form hydrogen bonds with key residues in the ligand-binding core. Our data suggested, however, that the contribution of the C_8 hydroxy group to the stability of GluK1 and GluK2 complexes was clearly different. The C_8 hydroxy group in GluK2 had two hydrogen bonds with Glu707 (738) and Thr710 (741), whereas that in GluK1 only formed one hydrogen bond with Glu723 (738) (Table 2). Interestingly, no hydrogen-bonding interaction was detected between the C_8 hydroxy group of NDH and the Ser726 (741) residue in GluK1 that corresponds to Thr710 (741) in GluK2. This subtle difference was not predicted by MD simulation.[11,17]

Another interesting aspect in ligand binding between GluK2 resides in the orientation of Asn690 (721). Previously, Asn690 (721) was demonstrated to be a key residue that interferes with the binding of GluK1-selective ligands to GluK2 by steric occlusion.[17,21,28–30] Our crystal structure largely agreed with earlier predictions. However, a drastic rotation of the Asn690 (721) residue of GluK2 found in the crystal structure permitted NDH to enter the ligand-binding cavity. This conformational change disrupted important interdomain hydrogen bonding between Glu409 (441) and Asn690 (721), similar to that predicted for the GluK2-S1S2–MSVIII-19 complex.[17] This was unexpected because NDH functions as an efficacious agonist, and a firm hydrogen-bonding interaction between Glu409 (441) and Asn690 (721) was previously identified as an important determinant for a positive relationship between channel opening and domain closure.[17] Thus, the crystal structure of the hGluK2-S1S2–NDH complex suggested that, in GluK2, both domain closure and interdomain hydrogen bonding between Glu409 (441) and Asn690 (721) were not simply a determinant of the degree of channel opening. Smaller ligands, such as L-glutamate and kainate, did not induce this conformational change in Asn690 (721).[21]

In the present study, we found that deletion of the NDH C_9 hydroxy group caused conformational change in the associated ligand in binding complex with GluK1. 9-Deoxy-NDH was discovered in the twisted-boat form as a dominant conformation. This conformational change was attributed to the loss of an intramolecular hydrogen bond between the C_9 hydroxy group and the γ-carboxylate of the glutamate substructure in NDH (Fig. 4). This conformational change causes some loss of interactions within the GluK1 ligand-binding pocket, which reduce binding affinity for GluK1. However, lack of the steric occlusion by Asn690 (721), which was observed in GluK2, probably allowed binding of 9-deoxy-NDH with the twisted-boat form or of MSVIII-19 in a flattened conformation to GluK1. Moreover, approximately 10 hydrogen bonds formed tightly between GluK1 and the glutamate substructure can compensate for reduced affinity in the bicyclic portion. In contrast, these compounds are geometrically unfavorable for packing into GluK2-binding cavity unless Asn690 (721) is rotated. These observations concur with earlier findings.[11,17] In the crystal structure of the 9-deoxy-NDH complex, we observed the presence of a minor conformer in the extended bicyclic conformation, similar to MSVIII-19. It can thus be speculated that difference in ligand efficacy between 9-deoxy-NDH and

MSVIII-19 may underlie these structural differences; that is, if all 9-deoxy-NDH existed as only the "extended" conformation, then it would act as functional antagonist like MSVIII-19.

We also found that all of the NDH analogues investigated herein induced full domain closure, regardless of binding potency and agonist efficacy. This finding is consistent with the previously reported structures of DH and MSVIII-19 complexes.[17] It, however, differs with the observation in the domoate and kainate complexes with GluK2 where those partial agonists did not induce complete closure of the receptor.[31] Recently, twist motion between domain 1 and domain 2 was proposed as a factor that modulates channel opening efficacy upon ligand binding in GluA2.[27] Since Frydenvang *et al.* suggested additional factors underlying in the regulation of agonist efficacy in KAR,[17] we examined a series of ligand-bound GluK1 obtained in the present study for "twist" motion. Although slight differences in the motion between domain 1 and domain 2 relative to that of L-glutamate were detected, they were within the atomic resolution of the structure (Fig. 7). We therefore conclude that no significant twist motions exist when DH analogues bind to KAR ligand-binding core. This observation may suggest the following possibilities: (1) twist motion is not a factor that affects the agonist efficacy of DH for GluK1, and thus, some other mechanisms that govern the gating efficacy exist; (2) since DH stabilizes the desensitized state of the receptor so effectively, the crystal structures we obtained represent only a "snapshot" of the most stable ligand–receptor complex. Therefore, the "twist" motion may be still a possible factor, but it was not revealed in the crystal structures. Co-crystallization of DH analogues with non-desensitizing mutants of GluK1 would be necessary to clarify whether or not the motion of ligand-binding core is a factor for activating the channel.

Materials and Methods

DH analogues

DH and NDH were isolated from the marine sponge *L. chondrodes* as previously described by Sakai *et al.*[3,5] DH analogues, 8-deoxy-NDH, 9-deoxy-NDH and MSVIII-19, were synthesized as previously described.[7]

Protein expression

Constructs for expressing hGluK1-S1S2 and hGluK2-S1S2 were engineered in accordance with a procedure described previously.[22] S1 (415-ANRTL-ILYRK-529) and S2 (652-PIDSA-GNGCP-790) segments constituting that of hGluK1-S1S2 were amplified by polymerase chain reaction (PCR) from cDNA (human brain whole marathon ready; Clontech) using the following primers: S1-forward, ATTTGAATTCCGTGGTGCCAACAGAACACTCATTG; S1-reverse, ATTAGGTACCCTTCCGGTAGAGAATGC; S2-forward, ATTAGGTACCCCCATAGATTCGGCAGATG; and S2-reverse, AATTCTCGAGTTAGGGGCAGCCATTCCCA. Similarly, S1 (398-SNRSL-ILYRK-513) and S2 (636-PIDSA-NGCPE-775) segments constituting that of hGluK2-S1S2 were PCR amplified using the following primers: S1-forward, ACAGATGCTAGCTCCAATCGTTCTTTGATT; S1-reverse, TGTACCGGTACCCTTGCGGTACAAAATAC; S2-forward, CGCATGGGTACCCCTATTGACTCTGCTGAT; and S2-reverse, CTCTTTCTCGAGTTATTCTGGGCAACCATTG. PCR products were digested with EcoRI for the region corresponding to the hGluK1 N-terminus of S1 (NheI for hGluK2), with KpnI for regions corresponding to both the C-terminus of S1 and the N-terminus of S2 and with XhoI for the region corresponding to the C-terminus of S2, respectively. The digested insert was extracted and ligated with the pCold I DNA vector (TAKARA), which had been previously digested with EcoRI and SalI, since the pCold I DNA lacked a XhoI site. hGluK1-S1S2 was co-expressed with GroEL/ES using BL21(DE3) cells transformed by the chaperon plasmid pGro7 at 15 °C. Protein was successfully obtained from the supernatant after cell harvesting and centrifugation. Active hGluK2-S1S2 was successfully obtained only by co-expression with molecular chaperon. The sequences of the insert DNAs were verified by sequencing, and the expressed proteins were verified by matrix-assisted laser desorption/ionization–time of flight mass spectrometry. Expressed hGluK1-S1S2 and hGluK2-S1S2 sequences are numbered with respect to the first amino acid in the mature proteins.[21]

Protein purification

hGluK1-S1S2 was purified using an SP Sepharose high-performance (GE Healthcare) cation exchanger column with a linear gradient of 0–500 mM NaCl in 20 mM sodium phosphate buffer, pH 7.4. Following dialysis against 20 mM sodium phosphate buffer (pH 7.4), the protein was further purified by Ni^{2+} affinity chromatography using Ni-NTA agarose (QIAGEN) with a linear gradient of 0–500 mM imidazole in 20 mM Tris–HCl, pH 7.4. After dialysis against 20 mM Tris–HCl (pH 7.4), the His-tag was cleaved off by adding trypsin to the solution so that the weight ratio of trypsin to proteins was 1500, and the solution was maintained at room temperature for 80 min. The reaction was stopped by adding phenylmethylsulfonyl fluoride (1.3 mM) and ethylenediaminetetraacetic acid (EDTA) (20 mM). hGluK1-S1S2 was further purified using SP Sepharose high performance and Ni-NTA agarose, from which the flow-through fraction was collected for crystallization.

hGluK2-S1S2 was purified by a procedure similar to that for hGluK1-S1S2. However, in this case, the purification buffer contained 1 mM sodium hydrogen L-glutamate monohydrate, and thrombin was used instead of trypsin for His-tag digestion.

Crystallization

C2 crystals were obtained for complexes with L-glutamate, DH and NDH. Protein (5–15 mg/mL) was

dialyzed against a buffer containing 20 mM Hepes (pH 7.0), 30 mM NaCl and 1.0 mM EDTA. Crystals were obtained at 6 °C in hanging drops containing 2 μL protein and 2 μL reservoir solution, consisting of 13–23% polyethylene glycol (PEG) 3350, 10 mM citrate (pH 4.8), 1.0 M β-mercaptoethanol and 1–10 mM ligands (L-glutamate, DH or NDH). Crystals were grown for 5 days. Crystals were then transferred through a cryoprotectant with 18% glycerol in reservoir solution prior to flash-cooling in a cold nitrogen stream. *P*1 crystals were obtained for all ligand complexes reported herein. For crystallization, protein was concentrated to 2–3 mg/mL in a buffer containing 20 mM Hepes (pH 7.0), 30 mM NaCl and 1.0 mM EDTA. Crystals were obtained at 30 °C in hanging drops containing 2 μL protein solution and 2 μL reservoir solution, consisting of 25% PEG 3350, 0.3 M Li_2SO_4, 0.2 M 2-[bis(2-hydroxyethyl)amino]-2-(hydroxymethyl)propane-1,3-diol (pH 5.5) and 2–30 mM ligands. Only for the MSVIII-19 complex crystals, 1 mM aspartic acid was added to the reservoir solution.

In order to crystallize hGluK2-S1S2 in complex with NDH, the protein was concentrated to 5–15 mg/mL in a buffer containing 2 mM Tris–HCl (pH 8.0), 20 mM NaCl, 1.0 mM EDTA and 10 mM sodium L-aspartate monohydrate. Crystals were obtained at 30 °C in hanging drops containing 2 μL protein solution and 2 μL reservoir solution, consisting of 40% PEG 4000, 1 mM EDTA, 10 mM NaCl, 2 mM Tris, 1.25 mM glutathione, 1.25 mM glutathione disulfide and 50–300 mM NDH adjusted to pH 4.6.

Data collection

X-ray diffraction data were collected at 100 K using an oscillation method (1.0° per frame) in synchrotron facilities using beamlines, detectors, camera distance, exposure time per frame and wavelength listed in Table S1. Data for BL26B1 and BL26B2 were obtained using mail-in service. The HKL-2000 package[32] was used for auto-indexing and data processing. For statistics, see Table S1.

Structure determinations and refinements

The L-glutamate complex of the hGluK1-S1S2 structure (type I) was first determined by the molecular replacement method using the *CNS* program package.[33,34] The structure of the rat GluK1-S1S2 (GluR5-S1S2) in complex with L-glutamate (PDB ID 1txf)[21] was used as a search model, from which L-glutamate and water molecules were omitted. Manual model building and correction were performed with the program Coot.[35] Initial model refinements and calculations were carried out with the *CNS* program with iterative cycles of simulated annealing and individual *B*-factor refinements. After several refinement cycles, water molecules, SO_4^{2-} ions, β-mercaptoethanol and L-glutamate were added to the model. The model was further refined using the maximum-likelihood target with the program REFMAC5.[36] After the introduction of alternative conformations for several residues and the translation–liberation–screw refinement,[37] the final *R* and R_{free} factors dropped to 20.1% and 24.5%, respectively.

The structure of the hGluK1-S1S2–L-glutamate complex was used as a search model in order to determine the structures of DH and NDH complexes (in *C*2 crystals). These structures were refined using the same procedure as that performed for the L-glutamate complex. Molecular structures of the ligands and the dictionaries used for successive calculations were produced by the PRODRG server.[38] Model reconstruction of the compounds were carried out with TURBO-FRODO.[39]

Structures of the complexes with the DH analogues and the L-glutamate complex in the *P*1 s.g. were determined by the molecular replacement method using the DH complex of the hGluK1-S1S2 structure as a search model. All *P*1 crystals contained two molecules of hGluK1-S1S2 in the a. u. After determining the initial phase, structures were refined by the same procedure. The C-terminal region between Arg785 (800) and Gly788 (803) was disordered; thus, only main chains were modeled [Cys789 (804) and Pro790 (805) were unambiguously determined].

Finally, the NDH complex of the hGluK2-S1S2 structure was determined by the molecular replacement method using the structure of the rat GluK2-S1S2 (GluR6-S1S2) in complex with L-glutamate (PDB ID 3g3f) as the initial model. The structure was refined using the same procedure. Refinement statistics are listed in Table S1.

Accession numbers

Coordinates of hGluK1-S1S2 have been submitted to the PDB [2ZNS for the L-glutamate complex (s.g. *C*2), 2ZNT for the DH complex (s.g. *C*2), 2ZNU for the NDH complex (s.g. *C*2), 3FUZ for the L-glutamate complex (s.g. *P*1), 3FV1 for the DH complex (s.g. *P*1), 3FV2 for the NDH complex (s.g. *P*1), 3FVG for the MSVIII-19 complex, 3FVK for the 8-deoxy-NDH complex and 3FVN for the 9-deoxy-NDH complex of GluK1-S1S2]. Coordinates of hGluK2-S1S2 in complex with NDH is submitted as 3QXM.

Acknowledgements

This work has been supported in part by a project grant from the Institute of Multidisciplinary Research for Advanced Material, Tohoku University (to M.U.); the Management Expenses Grants for National Universities Corporations (to M.I.-S.) from Ministry of Education, Culture, Sports, Science and Technology, Japan; and Grants-in-Aid for Scientific Research 20770076, 18032012 (to M.U.) and 16073202 (to M.S.) from Japan Society for the Promotion of Science and Ministry of Education, Culture, Sports, Science and Technology, Japan. Synchrotron radiation experiments were performed at BL44B2, BL26B1 and BL26B2 (RIKEN beamlines) of SPring-8 and at BL5A, BL17A, NE3A and NW12A of Photon Factory and Photon Factory Advanced Ring under the approval of 2007G515, 2007G516 and 2009G501.

Supplementary Data

Supplementary data to this article can be found online at doi:10.1016/j.jmb.2011.08.043

References

1. Hollmann, M. & Heinemann, S. (1994). Cloned glutamate receptors. *Annu. Rev. Neurosci.* **17**, 31–108.
2. Swanson, G. T. & Sakai, R. (2009). Ligands for ionotropic glutamate receptors. *Prog. Mol. Subcell. Biol.* **46**, 123–157.
3. Sakai, R., Kamiya, H., Murata, M. & Shimamoto, K. (1997). Dysiherbaine: a new neurotoxic amino acid from the Micronesian marine sponge *Dysidea herbacea*. *J. Am. Chem. Soc.* **119**, 4112–4116.
4. Sakai, R., Swanson, G. T., Shimamoto, K., Green, T., Contractor, A., Ghetti, A. *et al.* (2001). Pharmacological properties of the potent epileptogenic amino acid dysiherbaine, a novel glutamate receptor agonist isolated from the marine sponge *Dysidea herbacea*. *J. Pharmacol. Exp. Ther.* **296**, 650–658.
5. Sakai, R., Koike, T., Sasaki, M., Shimamoto, K., Oiwa, C., Yano, A. *et al.* (2001). Isolation, structure determination, and synthesis of neodysiherbaine A, a new excitatory amino acid from a marine sponge. *Org. Lett.* **3**, 1479–1482.
6. Swanson, G. T., Green, T., Sakai, R., Contractor, A., Che, W., Kamiya, H. & Heinemann, S. F. (2002). Differential activation of individual subunits in heteromeric kainate receptors. *Neuron*, **34**, 589–598.
7. Shoji, M., Akiyama, N., Tsubone, K., Lash, L. L., Sanders, J. M., Swanson, G. T. *et al.* (2006). Total synthesis and biological evaluation of neodysiherbaine A and analogues. *J. Org. Chem.* **71**, 5208–5220.
8. Sasaki, M., Tsubone, K., Shoji, M., Oikawa, M., Shimamoto, K. & Sakai, R. (2006). Design, total synthesis, and biological evaluation of neodysiherbaine A derivative as potential probes. *Bioorg. Med. Chem. Lett.* **16**, 5784–5787.
9. Sakai, R., Swanson, G. T., Sasaki, M., Shimamoto, K. & Kamiya, H. (2006). Dysiherbaine: a new generation of excitatory amino acids of marine origin. *Cent. Nerv. Syst. Agents Med. Chem.* **6**, 83–108.
10. Sasaki, M., Tsubone, K., Aoki, K., Akiyama, N., Shoji, M., Oikawa, M. *et al.* (2008). Rapid and efficient synthesis of dysiherbaine and analogues to explore structure–activity relationships. *J. Org. Chem.* **73**, 264–273.
11. Lash, L. L., Sanders, J. M., Akiyama, N., Shoji, M., Postila, P., Pentikainen, O. T. *et al.* (2008). Novel analogs and stereoisomers of the marine toxin neodysiherbaine with specificity for kainate receptors. *J. Pharmacol. Exp. Ther.* **324**, 484–496.
12. Sanders, J. M., Ito, K., Settimo, L., Pentikainen, O. T., Shoji, M., Sasaki, M. *et al.* (2005). Divergent pharmacological activity of novel marine-derived excitatory amino acids on glutamate receptors. *J. Pharmacol. Exp. Ther.* **314**, 1068–1078.
13. Sasaki, M., Maruyama, T., Sakai, R. & Tachibana, K. (1999). Synthesis and biological activity of dysiherbaine model compound. *Tetrahedron Lett.* **40**, 3195–3198.
14. Lomeli, H., Wisden, W., Köhler, M., Keinänen, K., Sommer, B. & Seeburg, P. H. (1992). High-affinity kainate and domoate receptors in rat brain. *FEBS Lett.* **307**, 139–143.
15. Gregor, P., O'Hara, B. F., Yang, X. & Uhl, G. R. (1993). Expression and novel subunit isoforms of glutamate receptor genes GluR5 and GluR6. *NeuroReport*, **4**, 1343–1346.
16. Qiu, C. S., Lash-Van Wyhe, L., Sasaki, M., Sakai, R., Swanson, G. T. & Gereau, R. W., IV (2011). Antinociceptive effects of MSVIII-19, a functional antagonist of the GluK1 kainate receptor. *Pain*, **152**, 1052–1060.
17. Frydenvang, K., Lash, L. L., Naur, P., Postila, P. A., Pickering, D. S., Smith, C. M. *et al.* (2009). Full domain closure of the ligand-binding core of the ionotropic glutamate receptor iGluR5 induced by the high affinity agonist dysiherbaine and the functional antagonist 8,9-dideoxyneodysiherbaine. *J. Biol. Chem.* **284**, 14219–14229.
18. Madden, D. R. (2002). The structure and function of glutamate receptor ion channels. *Nat. Rev., Neurosci.* **3**, 91–101.
19. Armstrong, N., Sun, Y., Chen, G. Q. & Gouaux, E. (1998). Structure of a glutamate-receptor ligand-binding core in complex with kainate. *Nature*, **395**, 913–917.
20. Armstrong, N. & Gouaux, E. (2000). Mechanisms for activation and antagonism of an AMPA-sensitive glutamate receptor: crystal structures of the GluR2 ligand binding core. *Neuron*, **28**, 165–181.
21. Mayer, M. L. (2005). Crystal structures of the GluR5 and GluR6 ligand binding cores: molecular mechanisms underlying kainate receptor selectivity. *Neuron*, **45**, 539–552.
22. Naur, P., Vestergaard, B., Skov, L. K., Egebjerg, J., Gajhede, M. & Kastrup, J. S. (2005). Crystal structure of the kainate receptor GluR5 ligand-binding core in complex with (*S*)-glutamate. *FEBS Lett.* **579**, 1154–1160.
23. Sanders, J. M., Pentikainen, O. T., Settimo, L., Pentikainen, U., Shoji, M., Sasaki, M. *et al.* (2006). Determination of binding site residues responsible for the subunit selectivity of novel marine-derived compounds on kainate receptors. *Mol. Pharmacol.* **69**, 1849–1860.
24. Sommer, B., Burnashev, N., Verdoorn, T. A., Keinanen, K., Sakmann, B. & Seeburg, P. H. (1992). A glutamate receptor channel with high affinity for domoate and kainate. *EMBO J.* **11**, 1651–1656.
25. Hayward, S. & Lee, R. A. (2002). Improvements in the analysis of domain motions in proteins from conformational change: DynDom version 1.50. *J. Mol. Graphics Modell.* **21**, 181–183.
26. Postila, P. A., Swanson, G. T. & Pentikainen, O. T. (2010). Exploring kainate receptor pharmacology using molecular dynamics simulations. *Neuropharmacology*, **58**, 515–527.
27. Birdsey-Benson, A., Gill, A., Henderson, L. P. & Madden, D. R. (2010). Enhanced efficacy without further cleft closure: reevaluating twist as a source of agonist efficacy in AMPA receptors. *J. Neurosci.* **30**, 1463–1470.
28. Swanson, G. T., Green, T. & Heinemann, S. F. (1998). Kainate receptors exhibit differential sensitivities to (*S*)-5-iodowillardiine. *Mol. Pharmacol.* **53**, 942–949.
29. Swanson, G. T., Kamboj, S. K. & Cull-Candy, S. G. (1997). Single-channel properties of recombinant AMPA receptors depend on RNA editing, splice variation, and subunit composition. *J. Neurosci.* **17**, 58–69.